

Meteorological scenario of Ethiopian floods in 2006–2007

Mark R. Jury

Received: 22 March 2010 / Accepted: 29 August 2010 / Published online: 16 September 2010
© Springer-Verlag 2010

Abstract The meteorological scenario of Ethiopian highlands floods is studied. Daily rainfall in the period 1997–2007 reveals two peaks: 23–28 July 2006 and 26–31 July 2007. National Center for Environmental Prediction (NCEP) composites suggest that anomalous southerly monsoon flow over the West Indian Ocean is re-directed by an anomalous Arabian ridge westward across the Red Sea and Ethiopia. A tongue of moisture stretches from the Congo towards the highlands, but westerly equatorial wind anomalies are absent. Anomalous sinking motions and dry conditions are evident over the West Indian Ocean. Diurnal analysis reveals northwesterly flow over eastern Sudan during afternoon hours, whilst back-trajectory analysis highlights a Red Sea source and lifting over the eastern escarpment of Ethiopia. The upper level tropical easterly jet connects Indian and Ethiopian rainfall at intra-seasonal (~40 days) time scale; whilst low-level meridional flow convergence is evident during flood events. Hovmoller analysis on 10°N reveals cyclonic signals propagating westward from the Arabian Sea at 500 km day^{-1} that produces a 10-day cycle in Ethiopian rainfall. The floods in 2006–2007 occurred at the peak of the annual cycle, with diurnal controls inducing $\frac{3}{4}$ of rain in the late evening. Whilst cold surges from southern Africa played a role in the 2006 flood, bursts in the northern Hadley cell are a more general determinant. The convection associated with the 2007 flood went on to become a destructive Atlantic hurricane.

1 Introduction

Although Africa is often plagued by drought, heavy rainfall in 2006 and 2007 over the Ethiopian highlands (6–14°N, 35–40°E; Fig. 1a, b) caused flooding of the Blue Nile River. The Ethiopian Meteorological Service reported July totals >400 mm across western districts, with daily totals >100 mm and seasonal totals up to 2,000 mm (Table 1). The United Nations reported 620 fatalities, ~35,000 displaced and ~118,000 people ‘affected’ by flooding in 2006. During 2007, floods again spread across the region with ~20,000 displaced and ~103,000 affected. All major rivers overflowed and drainage into Sudan resulted in 122 fatalities and ~200,000 homeless. The floods destroyed crops and livestock across Northeast Africa, where most people depend on farming for their livelihoods. The World Health Organization reported in September 2007 that ~3.5 million people along the Sudan–Ethiopian border were at risk of flood-related epidemics, such as dysentery and malaria.

Wegiel and Herbster (1998) and Hill and Lin (2003) have demonstrated how convective outbreaks over the Ethiopian highlands form into African easterly waves. Through satellite imagery, synoptic observations and model simulations, evening thunderstorm clusters merge into a vortex downstream over Sudan and propagate westward. Hill and Lin (2003) characterized the meteorological conditions over the Ethiopian highlands in late July 2000 as having favorable horizontal and vertical easterly wind shear (relative vorticity $>10^{-4} \text{ s}^{-1}$) and equivalent potential temperature $>345 \text{ K}$ in the 850–300 hPa layer induced by moist inflows from southern Sudan and the Red Sea. Matthews (2004) identified zonal propagating intertropical waves as a source of cyclonic shear on the equatorward flank of the African easterly jet, leading to enhanced convection at synoptic and intra-seasonal time

M. R. Jury
Physics Department, University of Puerto Rico,
Mayagüez 00681, Puerto Rico

M. R. Jury (✉)
University of Zululand,
KwaDlangezwa 3886, South Africa
e-mail: mark.jury@upr.edu

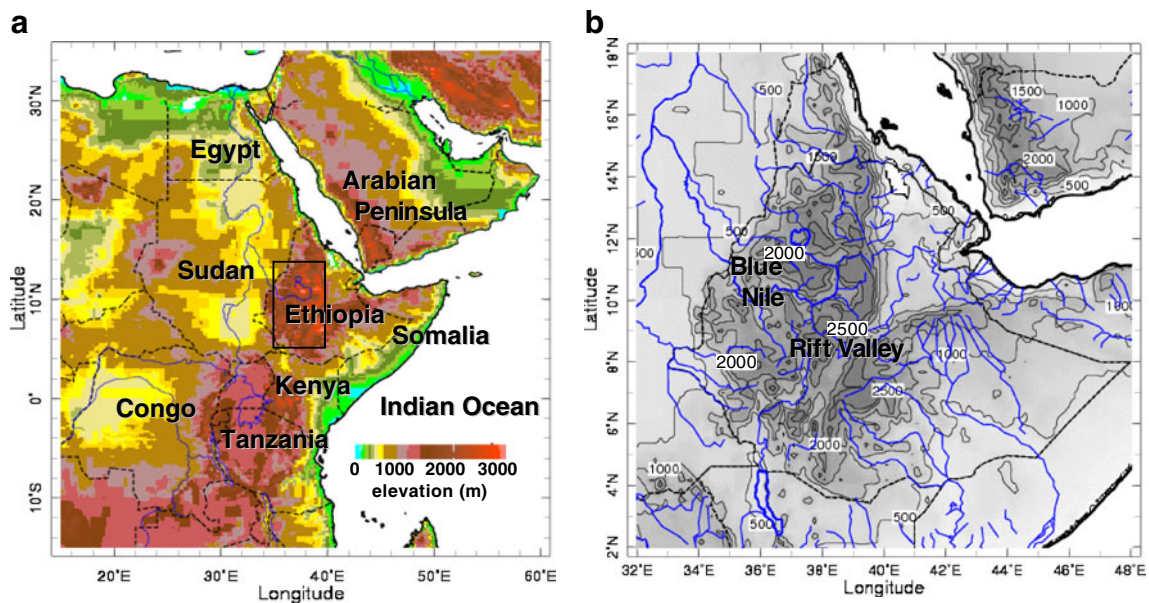


Fig. 1 (a) Topographic map of northeastern Africa with national borders; *box* outlines area used in statistical analyses. (b) Close-up view of Ethiopian highlands with shaded contours at 500 m and rivers (*blue*)

scales. Studies relating the regional meteorology to global climate have shown that Ethiopian rainfall and Blue Nile flow is enhanced by La Niña conditions and a more intense Indian monsoon (Camberlin 1997) which modulates the tropical circulation (Eltahir 1996; Potter et al. 2004; Korecha and Barnston 2007; Segele et al. 2009). The Atlantic zonal overturning circulation that often develops during Pacific La Niña has upper easterly/lower westerly flow that brings widespread uplift (descent) to Africa (South America), as outlined by Yeshanew and Jury (2007) and Jury (2009). Conway et al. (2004) and Seleshi and Camberlin (2006) studied daily rainfall records for Ethiopia and found little trend in extreme events, despite a weak down-trend in the Nile River flow in the 20th century (Conway et al. 2009). Heavy rains are an annual occurrence that generally benefit agriculture and water resources. Blue Nile flow from central Ethiopia (Fig. 1b) is typically $\sim 50 \times 10^9$ m³/yr (Vowinkel and

Orvig 1979; Ahmed and Ismail 2008). About 30% of Blue Nile flow in Sudan derives from July rainfall over Ethiopia, with ~ 1 -month delay. Run-off efficiency averages $\sim 30\%$, whilst the coefficient of variability is $\sim 20\%$ (Dettinger and Diaz 2000). In 2006–2007, exceptional run-off contributed to numerous landslides and loss of infrastructure.

The objective of this paper is to understand the regional atmospheric circulation and thermodynamic conditions that modulated the 2006–2007 Ethiopian flood events through analysis of meteorological patterns on flood days and statistical analyses of filtered daily time series. It is hypothesized that a number of factors contribute to African flooding (Asnani 1993): (1) equatorial moisture is drawn from the Congo, (2) low-level winds undergo orographic and diurnal forcing, (3) the upper level tropical easterly jet (TEJ) surges in response to thermal gradients and (4) cold surges from southern Africa accelerate the southern Hadley

Table 1 Ethiopian highland station rainfall extremes for 2007 in descending rank

Station	Rainfall (mm/day)	Station	Rainfall (mm/season)
Gimbi ^a	116.8	Arjo ^b	1,940.5
Metema	103.9	Pawe	1,417.4
Assosa	102.5	Kachise	1,359.6
Adi Gudom	90.9	Bulen	1,354.0
Kibre Mengist	88.0	Gimbi	1,325.8
Chagni	82.6	Chagni	1,316.3
Bulen	75.1	Debre Tabor	1,314.4
Bahir Dar	74.1	Metema	1,240.7
Mankushe	73.2	Bahir Dar	1,132.3
Awassa	71.5	Nekemte	1,128.2

^a Position: 9°11'N, 35°50'E

^b 8°45'N, 36°30'E

Table 2 Cross-correlation of 3-day smoothed Ethiopian and Indian rainfall with various meteorological variables averaged over 6–14°N, 35–40°E in the period 1997–2007

	Eth-R	Prec. W	150 U	100 V	500 vort	700 Div	150 Div
Prec. W	0.68						
150 U	-0.56	-0.62					
700 V	-0.45	-0.36	0.64				
500 vort	0.38	0.42	-0.54	-0.50			
700 Div	-0.26	-0.42	0.21	0.12	-0.31		
150 Div	0.41	0.53	-0.37	-0.21	0.27	-0.49	
Ind-Rain	0.48	0.57	-0.74	-0.51	0.55	-0.22	0.31

Significant values ($r > |0.42|$) are in bold, after deflation of degrees of freedom for persistence. Parameter definitions: Prec. W, precipitable water; 150 U, 150 hPa zonal wind; 700 V, 700 hPa meridional wind; 500 vort, 500 hPa absolute vorticity; 700 Div, 700 hPa divergence; 150 Div, 150 hPa divergence

circulation. The statistical analysis seeks to establish the relative influence of different meteorological forcings, whilst composite, case study and Hovmoller analyses illustrate the regional atmospheric controls. This work will not delve into the wider issues of inter-annual variability

and hemispheric scale controls, but will instead focus on synoptic scale events over the Ethiopian highlands. In Section 2, the data and methods are outlined. Section 3 provides results in statistical context, as composites, and case studies. Conclusions are given in Section 4.

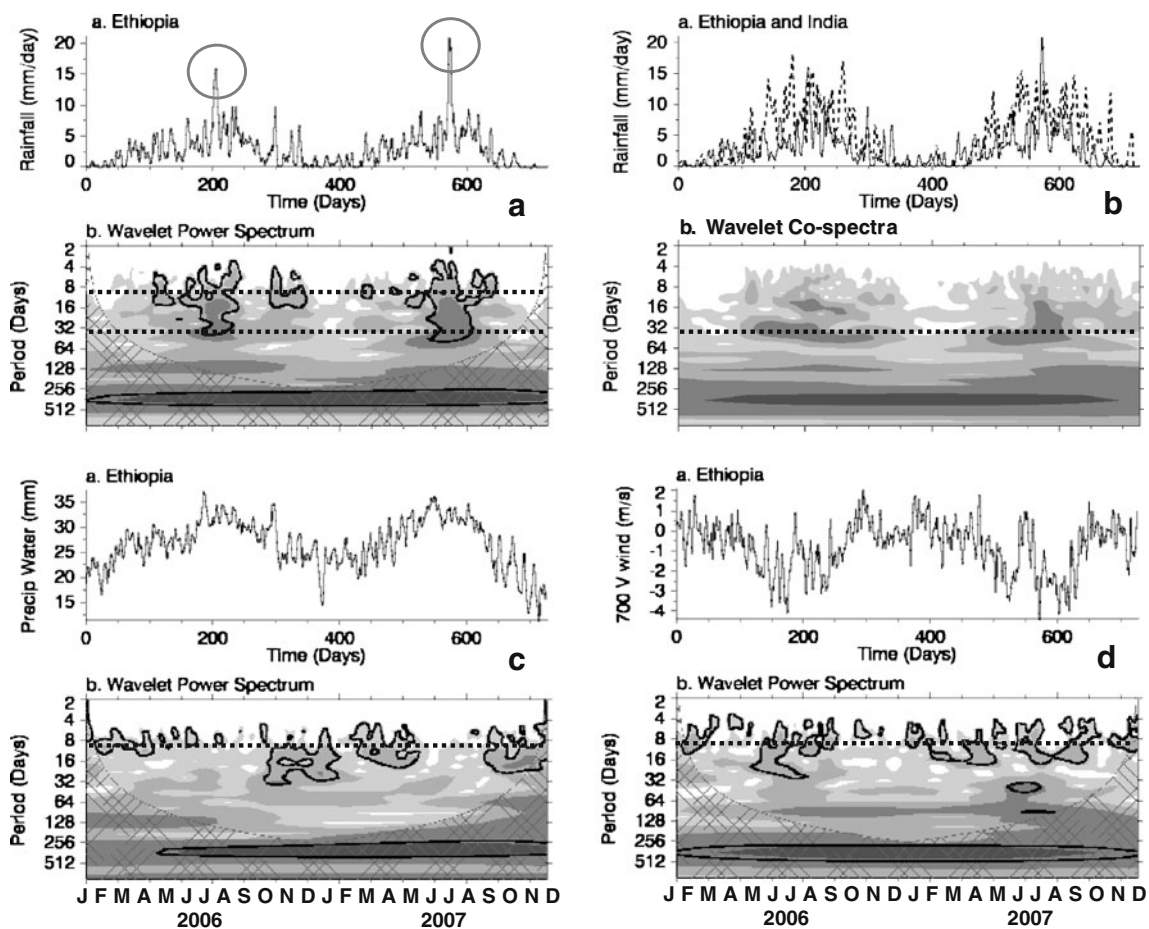


Fig. 2 Wavelet spectral analysis for 2006–2007 of **a** Ethiopian 3-day filtered rainfall, **b** co-spectra of Ethiopian and Indian monsoon rainfall, **c** Ethiopian precipitable water and **d** Ethiopian 700 hPa meridional wind. Energy is shaded at 25% power intervals; cone of validity given; outline

denotes statistical significance w.r.t. red noise at 90% confidence. Dashed lines highlight key cycles at 10 and 40 days; circles in **a** identify flood events: 23–28 July 2006 and 26–31 July 2007

2 Data and methods

To study flood events over the Ethiopian highlands, daily rainfall from the Global Precipitation Climatology Project (GPCP) was obtained in the period 1997–2007 as area averages: 6–14°N, 35–40°E via the International Research Institute (IRI) climate library (iridl.ldeo.columbia.edu). The GPCP rainfall product is based on satellite infrared radiance threshold as described by Adler et al. (2003), interpolated to a 1° grid. Rainfall data were similarly extracted over the Indian monsoon (10–25°N, 75–100°E) to explore the potential for intra-seasonal connections (Editorial MWR 1900; Hoyos and Webster 2007). Other rainfall data used here include the 3-hourly cMorph multi-satellite product (Joyce et al. 2004) and the daily Famine Early Warning System (FEWS) gauge-interpolated data (Love et al. 2004). The three rainfall products are consistent ($r > 0.80$) over the 2-year study period. Flood events were identified by

ranking 3-day area-averaged GPCP rainfall in the period 1997–2007 that contains diurnal and annual cycles.

To investigate the meteorological scenario, daily and 6-hourly re-analyzed 2° resolution atmospheric fields (Kanamitsu et al. 2002) from National Center for Environmental Prediction (NCEP) were obtained for the Ethiopian highland region: 700 hPa meridional wind, 150 hPa zonal wind, 500 hPa relative vorticity, 150 hPa divergence, 700 hPa divergence and precipitable water. Statistical associations between the area-averaged meteorological variables and Ethiopian 3-day rainfall in the period 1997–2007 were analyzed. Cross-correlation values $> |0.42|$ were deemed significant at 95% confidence, taking into account a reduced degrees of freedom from annual and synoptic cycles. The amplitude and period of oscillations in 2006–2007 were studied using wavelet spectral analysis, and statistical significance with respect to red noise was determined.

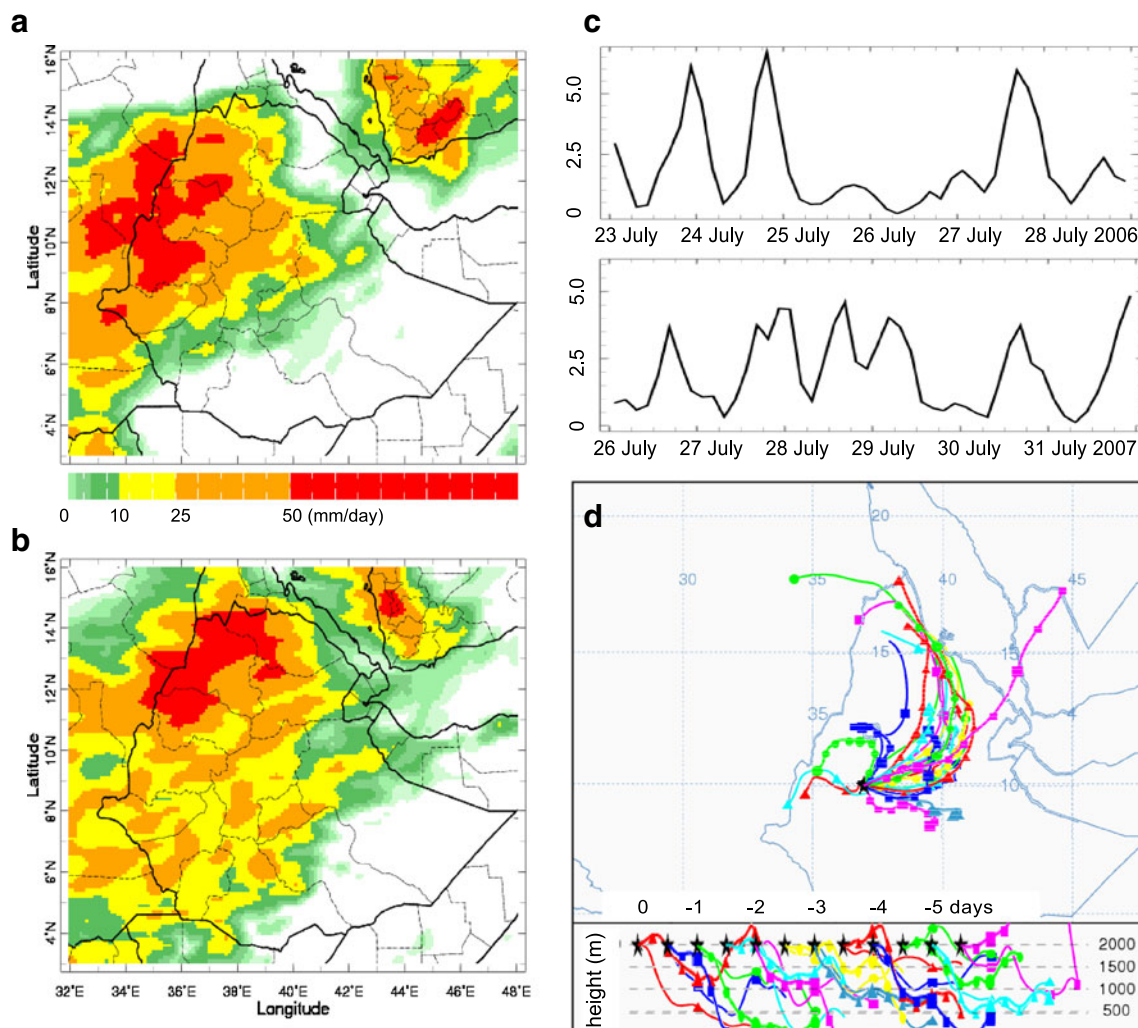


Fig. 3 Multi-satellite rainfall maps for **a** 23–28 July 2006, **b** 26–31 July 2007 and **c** their respective 3-h rainfall time series averaged over 6–14°N, 35–40°E. **d** Hysplit back-trajectory plan view and z - x section

analysis from 10°N, 37°E, 2,000 m above ground for two 5-day periods up to 27 July 2006 and 30 July 2007

After objectively ranking the Ethiopian highlands GPCP rainfall, two periods—23–28 July 2006 and 26–31 July 2007—had greatest rainfall. NCEP re-analysis fields for these 12 flood days were averaged, and the mean was subtracted to produce composite anomaly maps and cross-sections over Northeast Africa and the adjacent Indian Ocean 15°S–35°N, 15°E–60°E, following methods similar to those described by Fontaine et al. (1995) and Rudari et al. (2004). To study the diurnal cycle, 0800 hours LST fields were subtracted from 14:00 hours LST for surface air temperature and 700 hPa vector winds. Thus, the annual cycle was removed in the composites. Individual days within the two flood periods were further analyzed using 1° resolution Global Forecast System (GFS) numerical model analyses. Output fields for winds at 700 and 150 hPa, convergence, precipitable water, boundary layer height, convective available potential energy, surface air temperature and soil moisture were obtained, to understand localized and orographic forcing during peak floods. In addition, Hovmoller plots were drawn to understand temporal forcing and zonal wave propagation. cMorph rainfall estimates at 3-h intervals were analyzed for the two flood periods to quantify diurnal amplitude and air parcel back-trajectories were studied using the Hysplit model (<http://www.arl.noaa.gov/documents/reports/arl-224.pdf>) with an end-point at 10°N, 37°E, 2,000 m above ground from www.ready.noaa.gov. The methodology aims to provide a regional description of multi-variate factors contributing to Ethiopian flood events, and not to single out a certain influence, nor to imply cause–effect relationships.

3 Results

3.1 Statistical analysis of daily rainfall

Cross-correlations of 3-day filtered continuous Ethiopian highlands rainfall and meteorological variables in the period 1997–2007 are listed in Table 2. Values are significant (after deflation for annual cycle) for precipitable water, upper zonal wind, lower meridional wind and Indian monsoon rainfall. Indian rainfall generates the TEJ (Webster and Hoyos 2004) and modulates Ethiopian precipitable water, vorticity and meridional wind. Hence, the pulse frequency and amplitude of the Indian monsoon is connected with Northeast African highlands weather (Camberlin 1997). Conducting a stepwise multi-variate regression of all variables onto Ethiopian rainfall, precipitable water and 700 hPa meridional wind provide an optimal fit, $r^2=51\%$. The influence of meridional wind is negative, so pulses of northerly wind correspond with increased convection. These could be generated by interaction of the northern Hadley circulation and zonal propagating waves, as will be shown later.

The 2-year period 2006–2007 is analyzed for spectral energy for the leading variables in Fig. 2. Ethiopian highlands GPCP rainfall displays a seasonal increase with two sharp peaks at the end of July 2006 and July 2007 (Fig. 2a). Oscillations were significant about 10 days during the rainy season, and there was a low frequency pulse denoting the mid-summer maximum. One possible explanation for the 10-day cycle is intra-seasonal oscillations moving eastward across central Africa (Mutai and Ward 2000). Co-spectral energy between the Ethiopian and Indian rainfall

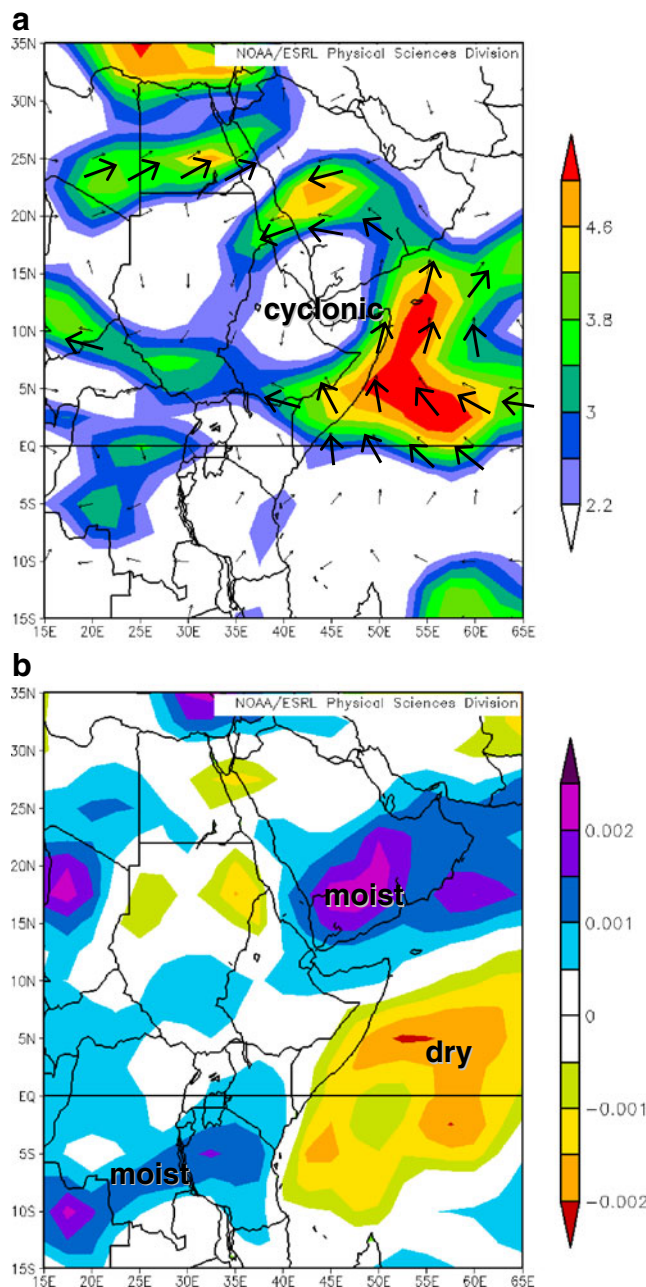


Fig. 4 Composite anomalies of National Center for Environmental Prediction (NCEP) reanalysis fields for 12 peak flood days in 2006–2007: **a** 700 hPa winds with bold arrows $>3 \text{ ms}^{-1}$, **b** 700 hPa specific humidity

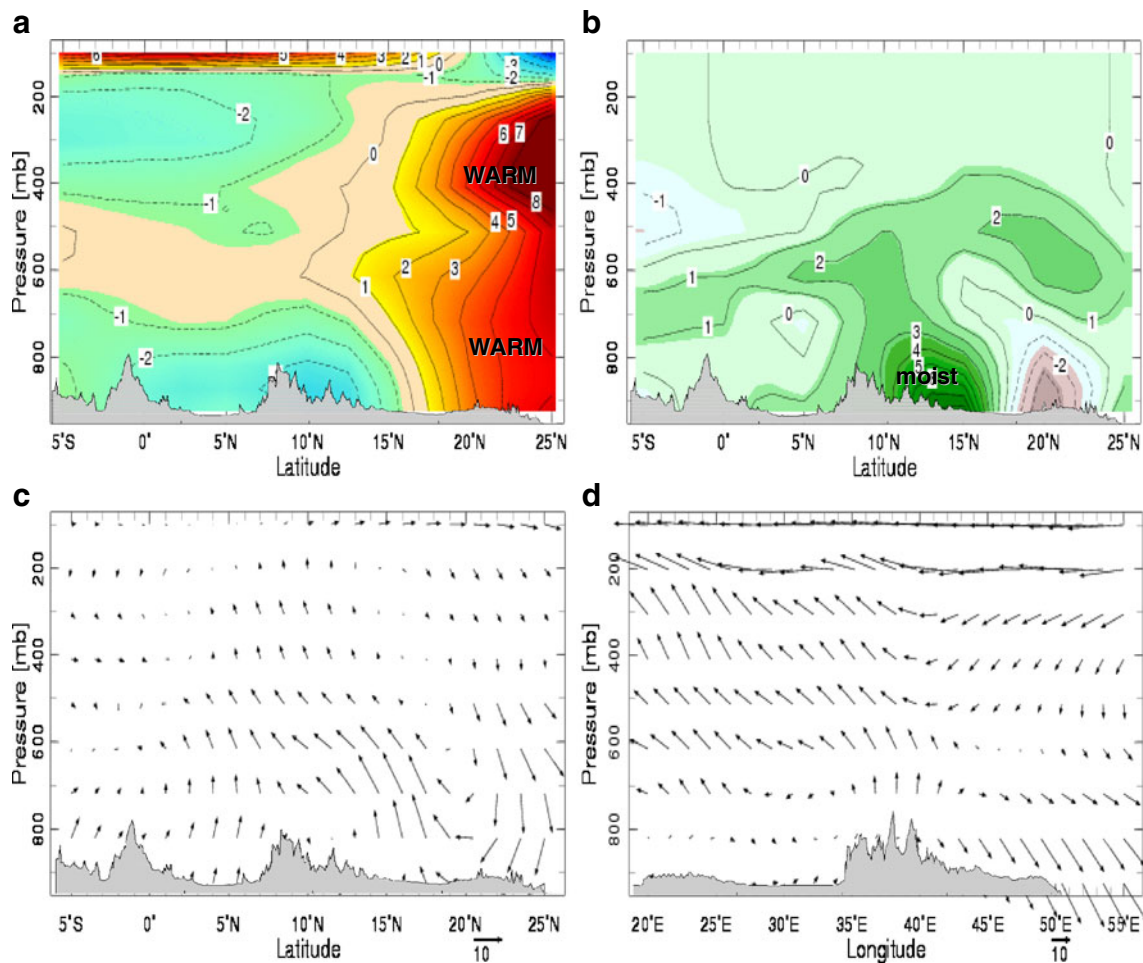


Fig. 5 Composite NCEP reanalysis fields for 12 peak flood days in 2006–2007 as vertical sections averaged over Ethiopian highlands: **a** temperature anomaly; **b** specific humidity anomaly; **c** V,W wind on north–south slice; **d** U,W wind on east–west slice. Vector key is given; W component $\times 10$

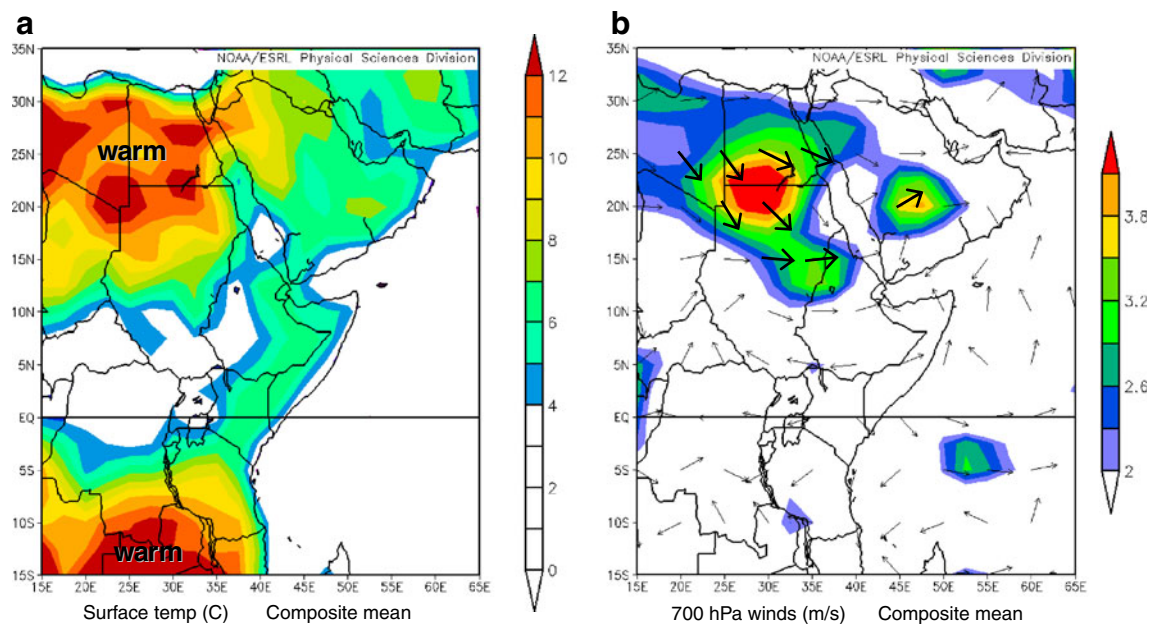


Fig. 6 Composite differences of NCEP reanalysis fields for 12 peak flood days in 2006–2007 describing diurnal amplitude (1,400 hours minus 0800 hours LST) for **a** 2 m air temperature and **b** 700 hPa winds with *bold arrows* $> 3 \text{ ms}^{-1}$

(Fig. 2b) was prominent around 40 days, suggesting the monsoon is modulated by Madden Julian Oscillations, which then ‘pulse’ the upper-level TEJ (Hulme and Tosdevin 1989; Rui and Wang 1990; Camberlin 1997; Hoyos and Webster 2007; Ding and Wang 2009). Both precipitable water and low-level meridional wind varied at intervals of about 10 days throughout the 2-year period (Fig. 2c, d).

cMorph rainfall for the two flood cases—23–28 July 2006 and 26–31 July 2007—is mapped in Fig. 3a, b. Highest rain rates occurred over western (2006) and northwestern (2007) Ethiopia, filling the Blue Nile River basin. Heavy rainfall extended into southeastern Sudan and the southwestern Arabian peninsula. The time series (Fig. 3c) indicate a pronounced diurnal cycle, with heaviest rainfall after 18:00 hours LST each day. The convection associated with the 2007 flood went on to become Hurricane Dean, a category 5 system that devastated parts of the Caribbean (www.nhc.noaa.gov/pdf/TCR-AL042007_Dean.pdf). The 2006 flood triggered an easterly wave that never intensified due to Saharan dust, amongst other factors. To determine air mass sources, Hysplit-model back-trajectories were analyzed from GFS analyses (Fig. 3d) using an ‘end point’ 2,000 m above ground (~700 hPa) at 10°N, 37°E. Two 5-day periods ending at 24:00 hours on 27 July 2006 and 30 July 2007 are considered. The majority of trajectories arrive from the Red Sea coast, following an anti-cyclonic arc over Eritrea. The *z*-*x* section of back-trajectories indicates that the channel leading into the Rift Valley (cf. Fig. 1b) funnels and lifts the flow in agreement with Kinuthia and Asnani (1982). Both 2006 and 2007 floods exhibit back-trajectories from the north; however, back-trajectory analysis for other Ethiopian floods (1998–2000) has inflow from the southwest (Congo).

3.2 Flood composite anomalies

Composite maps for flood days are given in Fig. 4. The 700-hPa wind anomalies exhibit a cyclonic vortex centered on Ethiopia (Fig. 4a). The southerly monsoon off the Somali coast is 5 ms⁻¹ stronger than usual, and draws easterly flow from the equatorial Indian Ocean. This anomalous flow extends toward the Arabian Peninsula and turns westward across the Red Sea then southward toward the Blue Nile catchment. Thus, part of the ‘Somali jet’ is briefly deflected back towards Africa. This appears to be a key process underlying the peak-season Ethiopian floods of 2006–2007. The 700 hPa specific humidity field (Fig. 4b) reveals anomalous dry conditions over the West Indian Ocean and enhanced moisture over the southern Arabian Peninsula/Gulf of Aden—a ‘source-sink’ pattern. Humid air also prevails from the Congo toward Kenya and Sudan. The composite anomaly ‘snap-shots’ indicate a cyclonic vortex over Ethiopia during the floods, whilst the

back-trajectories highlight northerly inflow as an important element in the precursor period.

Vertical section composite anomalies are shown in Fig. 5, based on NCEP re-analyses averaged on 32–37°E and 8–13°N. Temperatures exhibit a deep warm anomaly to the north (Fig. 5a) that strengthens the upper easterly jets. This warming reaches +6°C through the 800–300 hPa layer near 25°N (Egypt). Because of its structure, the warming is not only related to surface heating but indicative of an

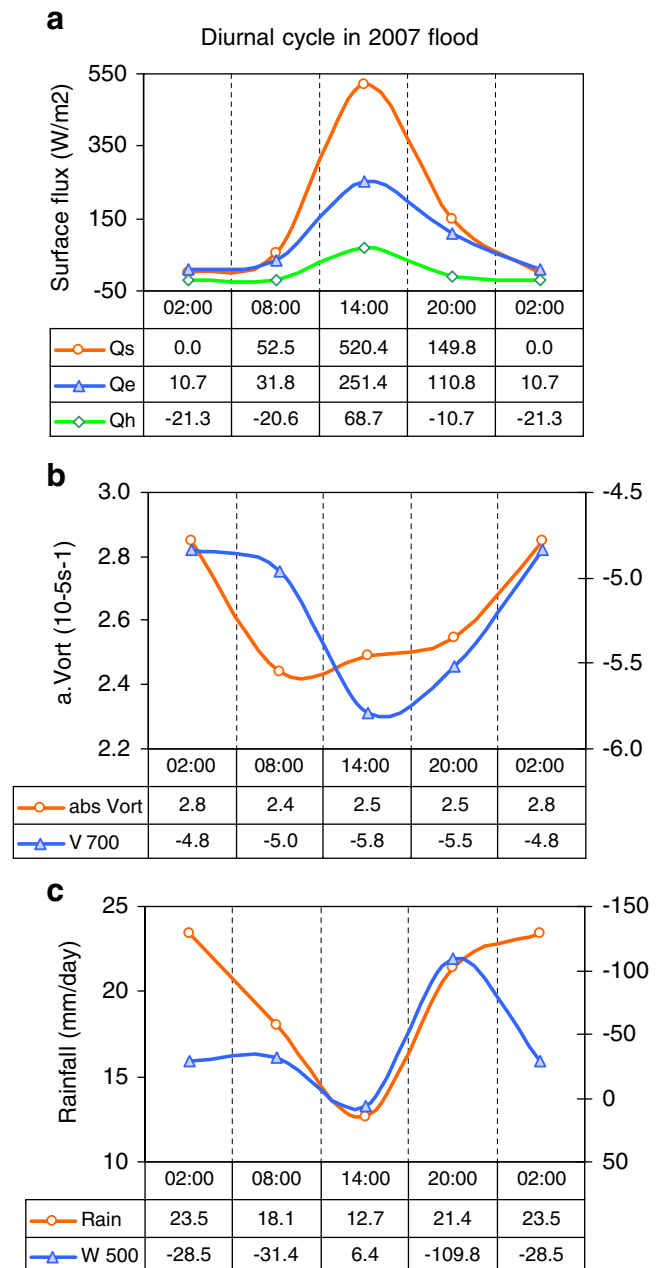


Fig. 7 Mean diurnal cycle in the period 24–31 July 2007 from 6-h NCEP reanalysis except for rainfall from cMorph product. **a** Surface fluxes: Qs insolation, Qe evaporation, Qh heat; **b** 500 hPa absolute vorticity (left) and 700 hPa meridional wind, and **c** rainfall (left) and 500 hPa vertical motion with Pa/s scale inverted

upper ridge over the eastern Mediterranean. Specific humidity increased over the equatorial zone and over the Ethiopian highlands from the surface up to 500 hPa. Moisture was depleted over Egypt as illustrated in the N–S section (Fig. 5b). The meridional wind and vertical motion pattern shows a tilted zone from 900 to 500 hPa of anomalous northerly rising flow (Fig. 5c) in the latitudes 10–17°N, consistent with the statistical results ($r=-0.45$ for 700 V, Table 2). Anomalous sinking motion over Egypt feeds into the northerly winds over Sudan. Zonal winds and vertical motions are analyzed as an east–west section in Fig. 5d. Anomalous rising motion prevails over the highlands and Sahel, as expected. Anomalous sinking motions are evident over the west Indian Ocean (55°E) particularly below 600 hPa. The TEJ accelerates downstream over Sudan. These circulation patterns are consistent with Hill and Lin (2003; their Fig. 5a) for easterly wave initiation over Ethiopia in July 2000.

Diurnal amplitude is studied on flood days by subtracting 0800 hours from 14:00 hours LST fields for 2 m air

temperature and 700 hPa winds; the resultant composite differences are mapped. Air temperatures increase 12°C over the northeastern Sahara desert (18–30°N) and the highlands of southern Africa (Fig. 6a). In the equatorial band 0–10°N, there is little change from morning to afternoon, according to NCEP re-analysis, due to clouds inhibiting surface heating and to evaporative cooling by rainfall. The wind response to diurnal heating is evident over southern Egypt and northern Sudan, with northwesterly differences $>3 \text{ ms}^{-1}$ (Fig. 6b) that enhance orographic lifting during afternoon hours along Ethiopia's NW border, consistent with back-trajectories (Fig. 3d) and the helical circulation (Fig. 5c).

The mean diurnal cycle was analyzed from 6-hourly NCEP re-analyses and cMorph rainfall, and results are presented for the 2007 flood event in Fig. 7. The diurnal cycle follows a sequence of (1) surface heating (insolation and heat fluxes $>800 \text{ W m}^{-2}$) by 14:00 hours LST (Fig. 7a), (2) deepening of the warm boundary layer $>2,000 \text{ m}$ above ground level (AGL) after 14:00 hours, causing an influx of northern flow (Fig. 7b). Cyclonic vorticity and vertical

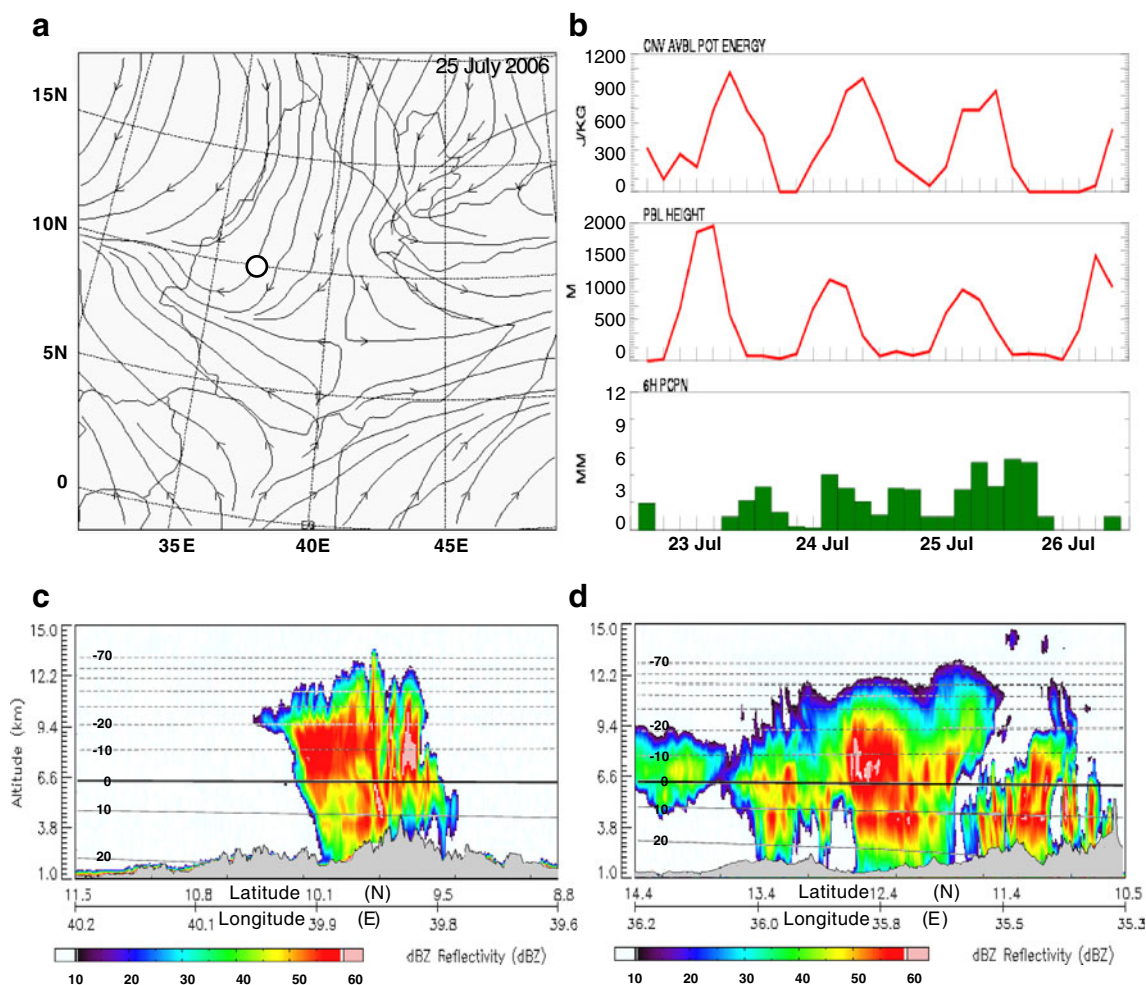


Fig. 8 a GFS 700 hPa wind streamlines for 18:00 hours LST 25 July 2006. b GFS meteorogram (at circle in a of CAPE, PBL height and 6-h rainfall in July 2006. CloudSat reflectivity slices on lines in e for 2,300 hours LST 24 July 2006 (c) and 1 August 2006 (d) with NCEP isotherms overlain

uplift are at a minimum during mid-day. (3) Towards sunset convective available potential energy rises and upward motions develop, (4) peak rainfall occurs from 2000 to 0200 hours (Fig. 7c) and corresponds with greater cyclonic vorticity. The late evening rainfall maximum is typical of continental highland locations in summer (Hill and Lin 2003; Singh and Nakamura 2009).

3.3 Analysis of July 2006 and July 2007 floods

The Blue Nile River in southeastern Sudan rose ~1 m after the floods, according to gauges at Roseries, Khartoum and Atbara. Meteorological features in the July 2006 flood are studied in Fig. 8a, b from GFS analyses. The 700-hPa wind streamline analysis of 18:00 hours LST 25 July reveals a classical neutral-point convergence, with southerly (northerly) flow over southern (northern) Ethiopia splitting eastward to the Indian Ocean and westward to the African Sahel. Meridional convergence in the lower levels was a significant factor in the floods. Above 500 hPa, flow was from ENE 20 m s^{-1} . The meteogram for the 3-day period (Fig. 8b) indicates a large diurnal cycle for planetary boundary layer (PBL) height and convective available potential energy (CAPE), with CAPE lagging >3-h with values up to $1,000 \text{ J kg}^{-1}$. Rainfall followed CAPE, peaking on the 25th. A total water volume $>10^{10} \text{ m}^3$ was generated for run-off by the end of July 2006. Satellite infrared imagery indicated that thunderstorm clusters reached -70°C over the western highlands following

earlier development along the eastern escarpment (disc.sci.gsfc.nasa.gov/hurricane/) and moved westward at $\sim 10 \text{ ms}^{-1}$. CloudSat reflectivity slices were collected at 23:00 hours LST on 24 July and 23:00 hours LST on 1 August 2006 (Fig. 8c, d) to describe the vertical structure of convection. In the first case, an isolated thunderstorm cluster developed near the eastern escarpment; in the second, a larger cluster was located over the NW border. There is high reflectivity above the freezing level indicative of cold cloud processes. Cluster diameters $>100 \text{ km}$ were typical. According to the GFS analysis of 18:00 hours LST 29 July 2007, surface air temperatures exceeded 35°C across the eastern lowlands of Ethiopia and Red Sea where the PBL lifted above 2,000 m. Over the highlands, surface temperatures remained near $\sim 15^\circ\text{C}$ and the PBL lifted $\sim 500 \text{ m}$. The eastern escarpment on 40°E divided the two regimes. Upper easterly winds of 40 ms^{-1} from 6° to 12°N coincided with upper divergence ($4 \times 10^{-4} \text{ s}^{-1}$). Soil moisture exceeded 40 mm over the highlands (not shown), helping to ‘anchor’ convective systems (Douville et al. 2001) and 700-hPa winds described a cyclonic vortex.

Hovmoller time-longitude plots were analyzed on $8\text{--}13^\circ\text{N}$ from daily GFS analyses, and the 2007 case is given in Fig. 9. The 700 hPa meridional wind anomaly pattern shows a steady increase of northerly flow over Ethiopia during the flood and a simultaneous acceleration of southerly winds to $\sim 10 \text{ ms}^{-1}$ over the West Indian Ocean (Fig. 9a). Westward propagation of 500 hPa vorticity anomalies is evident in Fig. 9b. A

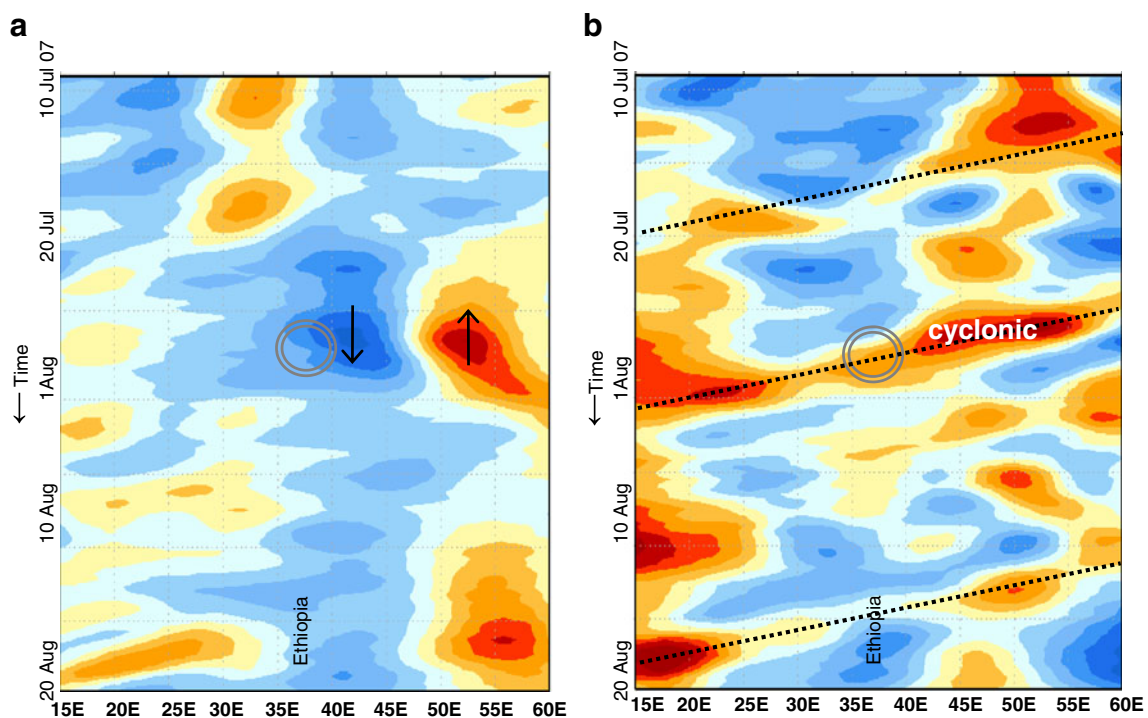


Fig. 9 Hovmoller plots averaged over $8\text{--}13^\circ\text{N}$ from 15 to 60°E for the period 10 July–20 August 2007. **a** 700 hPa meridional wind (shading blue -10 to red $+10 \text{ ms}^{-1}$), **b** 500 hPa relative vorticity (blue -5 to red $+5 \times 10^{-5} \text{ s}^{-1}$). Circle denotes flood event, dashed lines are cyclonic vortex propagation

cyclonic signal crosses the west Indian Ocean around 25 July 2007, moves over Ethiopia and Sudan during the flood event, and continues across the African Sahel at a speed of ~ 500 km day $^{-1}$. The passage of the system over Ethiopia caused low-level northerly winds to surge ($V \sim 7$ ms $^{-1}$), whilst upper easterly (U) winds oscillated from -15 to -30 ms $^{-1}$. In the 2006 case, a cyclonic signal propagating from the Arabian Sea is not so clear.

To understand whether cross-equatorial cold surges are important (Love 1985) to accelerating the southern Hadley circulation in Ethiopian floods, Hovmoller analyses were constructed for 700-hPa temperature, winds, vertical motion and rainfall averaged over the 30–35°E longitude from 40°S to 30°N and the case of 2006 is provided in Fig. 10. During the peak rains, a cold surge is seen to progress rapidly equatorwards as an area of increased southerly flow with $T < 15^\circ\text{C}$ between Zimbabwe and Kenya. Rainfall over Ethiopia follows rainfall near Durban, South Africa, as a cold front

passes, and is followed by a ridging anticyclone that delivers the cold air and accelerates the lower limb of the southern Hadley circulation. In the 2007 case, such a feature is not as obvious; instead, heavy rainfall extended southward into Kenya.

4 Conclusions

The analysis of daily Ethiopian highlands rainfall in the period 1997–2007 revealed two periods of flooding—23–28 July 2006 and 26–31 July 2007—that mark the seasonal peak of convection. Using NCEP composites, it was seen that anomalous southerly monsoon flow over the West Indian Ocean was re-directed westward across the Red Sea to Ethiopia. Inflow from the Congo did not play a role in these events. Instead, moisture was drawn from the West Indian Ocean, leaving anomalous sinking motions and dry

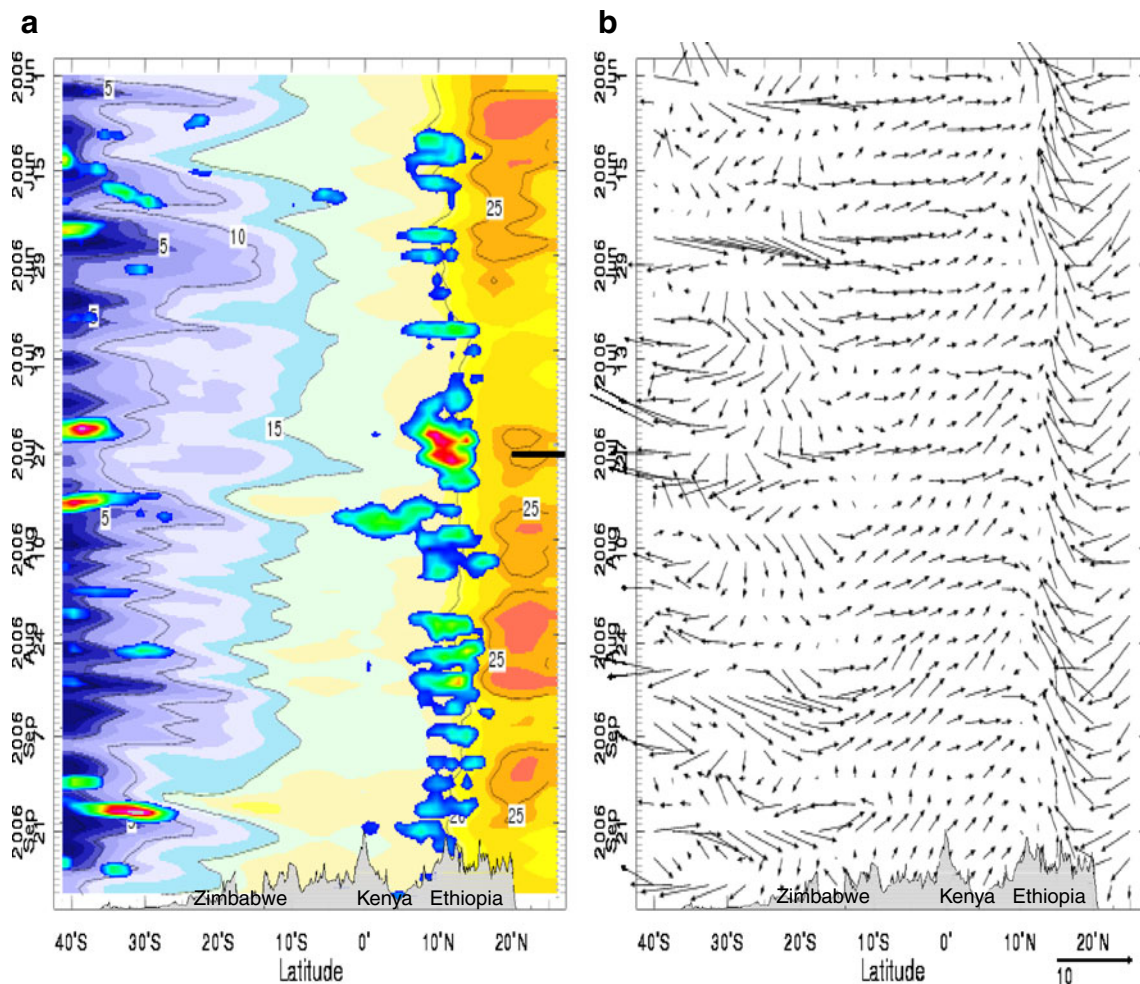


Fig. 10 Hovmoller plot averaged over 30–35°E from 40°S to 30°N for the period 1 June–30 September 2006 of **a** 850–700 hPa temperature (shaded blue to orange with contours at 5°C) and multi-satellite rainfall (rainbow shading aqua to red, 5 to 30 mm/day); and **b**

850–700 hPa meridional wind and 700–500 hPa vertical motion (largest vector = 5 ms $^{-1}$ with $W \times 10$). Topographic profile is plotted on lower axis. Bold tick highlights flood event.

conditions there. The diurnal analysis revealed additional northwesterly flow over Sudan during afternoon hours. Orographic forcing was evident in the back-trajectory analysis: re-directed monsoon flow passed over the Red Sea, funneled into the Rift Valley and lifted over the highlands of Ethiopia. The TEJ acts to connect Indian and Ethiopian rainfall at intra-seasonal time scales ($r=-0.74$, Table 2). Hovmoller analysis revealed cyclonic signals propagating westward from the Arabian Sea at ~ 500 km day⁻¹ (5.8 ms⁻¹) that pulse Ethiopian rainfall, precipitable water and meridional wind; and spawn African easterly waves (Hill and Lin 2003; Lin et al. 2005). The convection associated with the 2007 flood went on to become a destructive Atlantic hurricane. A key feature underlying the floods of 2006–2007 is a diurnally-modulated overturning circulation north of Ethiopia (cf. Fig. 5c) that represents a mid-summer burst of the northern Hadley cell in conjunction with a surge of the TEJ (Fig. 5d). Further work on Ethiopian flood events could include the use of in situ data and mesoscale model simulations, to distinguish annual, intra-seasonal, synoptic and diurnal factors.

Acknowledgments The author thanks Arba Minch University, Ethiopia, for stimulating this research.

References

Adler RF, Huffman GJ, Chang A, Ferraro R, Xie PP, Janowiak J, Rudolf B, Schneider U, Curtis S, Bolvin D, Gruber A, Susskind J, Arkin P, Nelkin E (2003) The Version-2 Global Precipitation Climatology Project (GPCP) monthly precipitation analysis (1979–present). *J Hydrometeorol* 4:1147–1167

Ahmed A, Ismail U (2008) Sediment in the Nile River system, UNESCO–IHP report, 93pp

Asnani GC (1993) Tropical meteorology. Noble Printers, Pune, 1202pp

Camberlin P (1997) Rainfall anomalies in the source region of the Nile and their connection with Indian summer monsoon. *J Clim* 10:1380–1392

Conway D, Mould C, Wolde AB (2004) One century of rainfall and temperature observations at Addis Ababa, Ethiopia. *Int J Climatol* 24:77–91

Conway D, Persechino A, Ardoin-Bardin S, Hamandawana H, Dieulin C, Mahé G (2009) Rainfall and water resources variability in sub-Saharan Africa during the twentieth century. *J Hydrometeorol* 10:41–59

Dettinger MD, Diaz HF (2000) Global characteristics of stream flow seasonality and variability. *J Hydrometeorol* 1:289–310

Ding Q, Wang B (2009) Predicting extreme phases of the Indian summer monsoon. *J Clim* 22:346–363

Douville H, Chauvin F, Broqua H (2001) Influence of soil moisture on the Asian and African monsoons. part I: mean monsoon and daily precipitation. *J Clim* 14:2381–2403

Editorial (1900) Nile floods and monsoon rains. *Mon Weather Rev* 28:324–325

Eltahir EA (1996) El Niño and natural variability in the flow of the Nile River. *Water Resour Res* 32:131–137

Fontaine B, Janicot S, Moron V (1995) Rainfall anomaly patterns and wind field signals over West Africa in August (1958–1989). *J Clim* 8:1503–1510

Hill CM, Lin Y-L (2003) Initiation of a mesoscale convective complex over the Ethiopian Highlands preceding the genesis of Hurricane Alberto (2000). *Geophys Res Lett* 30(5):1232. doi:10.1029/2002GL016655

Hoyos CD, Webster PJ (2007) The role of intra-seasonal variability in the nature of Asian monsoon precipitation. *J Clim* 20:4402–4424

Hulme M, Tosdevin N (1989) The tropical easterly jet and Sudan rainfall: a review. *Theor Appl Climatol* 39:179–187

Joyce RJ, Janowiak JE, Arkin PA, Xie PP (2004) cMorph: a method that produces global precipitation estimates from passive microwave and infrared data at high spatial and temporal resolution. *J Hydrometeorol* 5:487–503

Jury MR (2009) Ethiopian decadal climate variability. *Theor Appl Climatol* 98. doi:10.1007/s00704-009-0200-3

Kanamitsu M, Ebisuzaki W, Woollen J, Yang SK, Hnilo JJ, Fiorino M, Potter GL (2002) NCEP–DOE AMIP-II reanalysis (R-2). *Bull Am Meteorol Soc* 83:1631–1643

Kinuthia J, Asnani G (1982) A newly found jet in North Kenya (Turkana Channel). *Mon Weather Rev* 110:1722–1728

Korecha D, Barnston AG (2007) Predictability of June–September rainfall in Ethiopia. *Mon Weather Rev* 135:628–650

Lin YL, Robertson KE, Hill CM (2005) Origin and propagation of a disturbance associated with an African easterly wave as a precursor of Hurricane Alberto. *Mon Weather Rev* 133:3276–3298

Love G (1985) Cross-equatorial influence of winter hemisphere subtropical cold surges. *Mon Weather Rev* 113:1487–1498

Love TB, Kumar V, Xie P, Thiaw W (2004) A 20-year daily Africa precipitation climatology using satellite and gauge data. In Proc. 84th AMS Annual Meeting, Conference on Applied Climatology P5.4, Seattle

Matthews AJ (2004) Intraseasonal variability over tropical Africa during northern summer. *J Clim* 17:2427–2440

Mutai CC, Ward MN (2000) East African rainfall and the tropical circulation/convection on intraseasonal to interannual timescales. *J Clim* 13:3915–3939

Potter C, Zhang P, Klooster S, Genovese V, Shekhar S, Kumar V (2004) Understanding controls on historical river discharge in the world’s largest drainage basins. *Earth Interact* 8:1–21

Rudari R, Entekhabi D, Roth G (2004) Terrain and multiple-scale interactions as factors in generating extreme precipitation events. *J Hydrometeorol* 5:390–404

Rui H, Wang B (1990) Development characteristics and dynamic structure of tropical intraseasonal convection anomalies. *J Atmos Sci* 47:357–379

Segele ZT, Lamb PJ, Leslie LM (2009) Seasonal-to-interannual variability of Ethiopia/Horn of Africa monsoon: Part I. Associations of wavelet-filtered large-scale atmospheric circulation and global sea surface temperature. *J Clim* 22:3396–3421

Seleshi Y, Camberlin P (2006) Recent changes in dry spell and extreme rainfall events in Ethiopia. *Theor Appl Climatol* 83:181–191

Singh P, Nakamura K (2009) Diurnal variation in summer precipitation over the central Tibetan Plateau. *J Geophys Res* 114:D20107. doi:10.1029/2009JD011788

Vowinckel E, Orvig S (1979) The water budget and potential water reserves of the East Africa source region of the Nile. *J Appl Meteorol* 18:148–155

Webster PJ, Hoyos C (2004) Prediction of monsoon rainfall and river discharge on 15 to 30-day time scales. *Bull Am Meteorol Soc* 85:1745–1765

Wegiel, J. W., and C. G. Herbster, 1998. The origin of African easterly waves. In 16th Conf. Weather Analysis and Forecasting, Amer. Meteorol. Soc., Phoenix, Ariz

Yeshanew A, Jury M (2007) North African climate variability. Part 2. Tropical circulation systems. *Theor Appl Climatol*. doi:10.1007/s00704-006-0243-7